Catalysis Today, Volume 111, Issues 3-4, Pages 302-310

Running title; NO reduction on Pd(110)/ Ma & Matsushima

Surface-nitrogen removal in NO and N_2O reduction on Pd(110); Angular distribution studies of desorbing products

Yunsheng Ma and Tatsuo Matsushima*
Catalysis Research Center, Hokkaido University, Sapporo 001-0021, Japan (E-mail; tatmatsu@cat.hokudai.ac.jp)
* Corresponding author
(received; May 11, 2005, and revised form; July , 2005)

Abstract

This paper is a report of angle-resolved product desorption measurements in the course of catalyzed NO and N_2O reduction on Pd(110). Surface-nitrogen removal processes show different angular distributions, i.e., normally directed N_2 desorption takes place in process (i) $2N(a) \rightarrow N_2(g)$. Highly inclined N_2 desorption towards the [001] direction is induced in process (ii) $N_2O(a) \rightarrow N_2(g) + O(a)$. N_2O or NH_3 desorption follows the cosine distribution characterizing the desoptrion after the thermalization in process (iii) $N_2O(a) \rightarrow N_2O(g)$ or (iv) $N(a) + 3H(a) \rightarrow NH_3(a) \rightarrow NH_3(g)$. Thus, a combination of the angular and velocity distributions provides the analysis of most of surface-nitrogen removal processes in the course of catalyzed NO reduction.

At temperatures below 600 K, processes (ii) and (iii) dominate and process (iv) is enhanced at H_2 pressures higher than NO. Process (i) contributes significantly above 600 K. Only three processes except for NH_3 formation are operative when CO is used. Only process (ii) was observed in a steady-state N_2O+CO (or H_2) reaction.

Keywords; Nitrogen oxide, Nitrous oxide, Palladium, Single crystal surfaces, Reduction, Desorption

I. INTRODUCTION

The catalytic removal of nitrogen oxides from automobile exhaust has been achieved without definite knowledge of the reaction mechanism. The surface-nitrogen removal steps are still not clear because of the presence of several fast pathways after slow NO dissociation. Thus, a deep insight into the reaction mechanism will help us to improve the catalysts for the following generations. Angle-resolved (AR) product desorption measurements are useful for the analysis of surface-nitrogen removal in the course of a catalyzed NO reduction. This method is informative whenever any step becomes rate-determining because the angular distribution does not involve the reaction rate and is always related to the desorption process [1]. Fortunately, surface-nitrogen removal processes show different angular distributions of desorbing products, i.e., normally directed N_2 desorption takes place in the nitrogen associative process (i) $2N(a) \rightarrow N_2(g)$ [2-3]. Highly inclined N_2 desorption towards the [001] direction is induced in the intermediate N_2O decomposition process (ii) $N_2O(a) \rightarrow N_2(g) + O(a)$ [4-6]. N_2O or NH_3 desorption follows a broad cosine distribution in process (iii) $N_2O(a) \rightarrow N_2O(g)$ or (iv) $N(a) + 3H(a) \rightarrow NH_3(a) \rightarrow NH_3(g)$.

This paper reports AR-product desorption measurements in the course of the catalyzed NO and N_2O reduction on Pd(110). A combination of the angular and velocity distributions provides the analysis of all desorption processes involved in these catalyzed reactions [1]. The intermediate N_2O decomposition mostly shares the nitrogen removal pathway in the catalyzed NO + H_2 and NO + CO reactions below 600 K. Only three processes except for the NH_3 formation are operative when CO is used. The NH_3 formation is enhanced at H_2 pressures higher than that of NO.

II. EXPERIMENTS

The apparatus had three separately pumped chambers (Fig. 1) [1]. The reaction chamber was equipped with reverse-view low-energy electron diffraction (LEED) and X-ray photoelectron spectroscopy (XPS) optics, an ion gun, and a quadrupole mass spectrometer (QMS) for angle-integrated (AI) measurements. The chopper house, which had a large pumping rate of about 7 $m^3 \cdot s^{-1}$ for high angle resolution [7], had a narrow slit facing the reaction chamber and a cross-correlation chopper blade (see the insert in Fig. 1). Another QMS was set in the analyzer connected through a narrow tube for AR-product desorption and time-of-flight analyses. The distance from the ionizer to the chopper blade was 377 mm, and the selected time resolution was 20 μs.

^{15}NO (or $^{15}N_2O$) was introduced through a doser with a small orifice (diameter, 0.1 mm) about 2 cm from a sample crystal [8], while D_2 or ^{13}CO was backfilled. Hereafter, isotopes ^{15}N and ^{13}C are simply designated as N and C in the text, respectively. The product N_2, ND_3, CO_2, D_2O, and N_2O signals were monitored in both AI and AR forms. The desorption angle (polar angle, θ) was scanned in the plane along the [001] direction (see the insert in Fig. 1). The N_2 signals in both QMS's were corrected by the contribution due to the fragmentation of N_2O. The pressures of reactant gases were also corrected by their mass spectrometer sensitivities.

III. RESULTS

A. NO reduction

The steady-state NO reduction started around 500 K, was maximized around 530 K, and decreased at higher temperatures (Fig. 2). Below this optimum temperature, N_2 desorbed into inclined ways collimated around 41° off the surface normal toward the [001] direction. The intensity varied in a $\cos^{28}(\theta \pm 41)$ form where θ is the desorption angle (polar angle) (Fig. 3a). At higher surface temperatures, the normally directed N_2 desorption was enhanced (Fig. 3b). The observed desorption was deconvoluted by means of velocity analysis. No Maxwell distribution component at the surface temperature was found in the velocity curve of N_2 at the collimation angle below 540 K (Fig. 3c). The translational temperature calculated from the average kinetic energy was estimated to be 3540 K. Because of the wide distribution, the velocity curve was deconvoluted into two components in the way previously used [8]. The results are shown by broken curves. The resultant faster component reached 5810 K, and the slower one, 2200 K. On the other hand, the velocity curve at around 640 K significantly involved the Maxwell distribution component at the surface temperature, even at the collimation angle (Fig. 3d). This thermalized component was first subtracted and the resultant distribution was again deconvoluted into two components as shown by the broken curves in the figure. The desorption components at around 40° were identical to those from the inclined component at 530 K. This inclined component does not contribute the intensity at the normal direction as seen at 530 K (Fig.

3a). In fact, the velocity curve analysis at various desorption angles indicates that the faster component peaked at both the surface normal and the inclined direction. The flux followed a $\{\chi \cos^5\theta + \cos^{28}(\theta - 40)\}$ form where χ is a parameter indicating the relative intensity to the inclined component. The value increased with increasing surface temperature. The normally directed component is due to the associative desorption of nitrogen adatoms [2,3]. Neither angular nor velocity distribution is informative for the assignment of the thermalized component. The results from the steady-state N_2O reduction in the next chapter will show that the N_2O decomposition cannot yield the thermalized component. Thus, the thermalized component is likely to come from the associative process of nitrogen adatoms.

One of the products, D_2O, was desorbed in a cosine form and showed a Maxwell velocity distribution at the surface temperature, being identical to that in the $N_2O + D_2$ reaction in the next chapter (Fig. 4). The amount of the other product, ammonia, became significant when P_{D2} was higher than P_{NO}. The desorption of ammonia also showed a cosine angular distribution and the Maxwell velocity distribution at the surface temperature (Fig. 4a). These products are desorbed after thermalization to the surface temperature.

Only the (1×1) LEED pattern was observed in a $NO + D_2$ reaction at 5×10^{-8} Torr of NO with $P_{NO}/P_{D2} = 2$ and 450-800 K. The surface was in the reducing condition, yielding a non-reconstructed (1×1) form [9].

B. N_2O reduction

The steady-state N_2O reduction proceeded above 390 K when hydrogen or deuterium was used as a reducing reagent (Fig. 5a). The N_2 formation increased steeply with increasing surface temperature, reached a maximum at around 420 K and then decreased at higher temperatures. The starting temperature shifted to around 450 K when CO was used at $P_{CO} = 0.5\times10^{-6}$ Torr and increased steeply in a similar way to that with D_2 (Fig. 5b). The starting temperature decreased to around 400 K with decreasing P_{CO}, suggesting that the starting point was determined by the CO(a) removal. The product CO_2 desorption sharply collimated along the surface normal and its translational temperature was 1280 K at the normal direction (Fig. 4b). The velocity distribution involved the component from the Maxwellian distribution at the surface temperature. The fast component after subtraction of the thermalized one showed the translational temperature of 1610 K at the surface normal.

The angular distributionof desorbing N_2 became slightly broader at high temperatures from a $\cos^{28}(\theta - 45)$ form at 410 K to a $\cos^{19}(\theta - 46)$ form at 750 K (Fig. 6). The collimation angle was invariant in this temperature range. No changes were found in the velocity distributions in a wide temperature range although the signal intensity decreased significantly. Desorbing N_2 showed translational temperatures in the range of 2000 - 5000 K, identical to those in the $NO + D_2$ reaction below 550 K. Neither the cosine distribution nor the Maxwell distribution component at the surface temperature was found in desorbing N_2 in the N_2O reduction.

The reaction kinetics was switched at a critical CO/N_2O pressure ratio, 0.03 ~ 0.08, depending on the surface temperature (Fig. 7a). Below it (the active region), the reaction was a first order in CO and negative orders above it (the inhibited region). The reaction rate reached a constant value above the critical point when D_2 was used (Fig. 7b). The reaction clearly shows a switching of the rate-determining step from CO (or D_2) adsorption to N_2O adsorption at the critical point. Throughout the kinetic transition region, however, the N_2 desorption sharply collimated along 45º off the normal toward the [001] direction. No changes were found in the angular and velocity distributions of

desorbing N_2 below and above the critical point. This indicates that the desorption dynamics is merely controlled by its desorption process and not by the rate-determining step.

In the steady-state N_2O + CO reaction in the presence of 3×10^{-8} Torr of N_2O, a c(2×3)-1D-O LEED structure was observed when only N_2O was introduced and the intensity of the fractional order spots decreased with increasing CO pressure. Around the kinetic transition point and above it, the surface showed a clear (1×1) LEED pattern, suggesting that the surface was free of oxygen. The surface was again in the reducing condition, yielding a non-reconstructed (1×1) form [9].

C. Adsorbed species

The surface species was confirmed to change sharply at the critical pressure. The adsorbed species is O(a) or CO(a) for the N_2O + CO reaction because the reaction between CO(a) and O(a) is very fast and the amounts of N_2O(a) and N_2(a) must be very small in this temperature range because of their small heats of adsorption. This situation is very similar to that in the CO oxidation on noble metals. Thus, a pressure jump method can be applied to determine the amount of CO(a) and O(a) [10].

The typical decay curves of the AR-signals of N_2 at $\theta = 43°$ and CO_2 at $\theta = 0°$ are shown as a function of time after stopping of the CO supply (Fig. 8a). These curves were induced from the inhibited region above the kinetic transition. Both the N_2 and CO_2 signals showed a maximum. The CO_2 signal decreased quickly to the background after its maximum, whereas the N_2 signal decreased slowly. The peak area of N_2 before the maximum represents the amount of CO(a) after a proper sensitivity correction to the amount of CO_2, whereas that of N_2 after the maximum indicates the N_2 formation on an initially clean surface without removal of the deposited oxygen because of the fast reaction of CO(a) + O(a). Indeed, this N_2 was constant over the temperature range from 500 K to 400 K.

The peak area below the CO_2 curve represents the amount of CO(a) under the steady-state N_2O reduction, since the amount of CO adsorption after stopping of the CO supply was negligibly small and CO(a) is mostly removed as CO_2 below about 500 K [11]. The estimated CO(a) coverage was about one fourth of a monolayer at $T_S = 470$ K and $P_{CO} = 0.5\times10^{-6}$ Torr. The value was referred to the temperature-programmed desorption (TPD) curve from room temperature [12]. On the other hand, the area under the CO_2 decay curve from the active region was very small, i.e., the CO_2 signal quickly decreased without a maximum. Thus, the CO coverage jumped from a value of less than 0.05 monolayer (ML) to 0.25 ML at the critical pressure. It suggested that the surface is mostly covered by CO above the kinetic transition, and the amount of CO(a) affected the N_2O dissociation rate, whereas below the kinetic transition, the rate was affected by the amount of O(a).

We also examined the N_2 transient curves from the steady-state N_2O + D_2 reaction (Fig. 8b). The peak area induced from the D_2 pressure above the kinetic transition was close to that after the maximum above the transition in the N_2O + CO reaction, i.e., the surface was mostly clean, since the temperature was too high for hydrogen adsorption. The other product D_2O signal was very small because of the cosine distribution.

IV. DISCUSSION

A. Reaction pathways

The product N_2 is commonly emitted from N_2O(a) oriented along the [001] direction in both NO + D_2 (or CO) reaction below about 550 K and N_2O + D_2 (or CO) reaction. However, no N_2O(a) has been confirmed in the course of the catalyzed NO reduction by infrared reflection absorption spectroscopy (IRAS) and sum-frequency generation (SFG) [13,14]. In fact, the surface parallel N_2O must be insensitive toward the vibrational spectroscopy according to the surface selection rule [15]. Furthermore, the amount of N_2O would be very small above 400 K because of the small heat of adsorption. Both the desorption and dissociation of adsorbed N_2O are completed on Pd(110) below 160 K, showing a heat of adsorption less than 35 kJmole^{-1} [6]. At temperatures around 100 K, a standing form with the terminal nitrogen atom interacting with surface atoms was found by IRAS after exposure to N_2O [16]. However, this form is not the precursor of the inclined N_2 emission because oxygen is deposited on the surface in the N_2O(a) dissociation. In the inclined N_2 emission, the terminal oxygen atom must interact with the surface metal. A suitable lying form along the [001] direction as well as the standing form on the terminal nitrogen was recently proposed by density functional theory (DFT) calculations in a generalized gradient approximation level [17]. This lying form was predicted to be somewhat bent, bridging palladium-atom rows running along the [1$\bar{1}$0] direction.

Recent near-edge X-ray absorption fine-structure work at around 60 K also supports the presence of [001]-oriented N_2O from the remarkable anisotropy in the polarization dependence of the π resonance [18]. Furthermore, Watanabe recently reported in his STM work that isolated N_2O monomers were oriented along the [001] direction at 14 K although at 8 K, N_2O formed clusters extending along the [1$\bar{1}$0] direction [19]. The NCO(a) species found on Pd(111) and Pd(100) by IRAS [13,14] has no direct relation to N_2 desorption because the inclined N_2 desorption was observed even in the NO + D_2 reaction as well as in the NO + CO reaction. In other words, neither CO nor hydrogen is involved in the inclined N_2 desorption process. This was also confirmed from the observation of the same inclined N_2 emission in both N_2O + CO and N_2O + D_2 reactions.

Only the inclined N_2 desorption proceeds in the N_2O + D_2 (or CO) reaction in the wide temperature range studied, 400 – 800 K. Therefore, the themalized (cosine distribution) component of N_2 in the NO + D_2 (or CO) reaction should be formed in the other processes, probably in the associative process of N(a). The reason that desorbed N_2 from the associative process is largely thermalized is not currently clear. In the N_2O dissociation, the fragment N_2 is repulsed by the nascent O(a) which is more or less negatively charged on the metal surface. High repulsive forces may be operative between the resultant bulky ionic oxygen and the leaving N_2. Indeed, a large amount of energy, about 250 kJmol^{-1}, is released in the event of N_2O(a) $\rightarrow$ N_2(g) + O(a) [1,20]. On the other hand, in the event of N(a) + N(a) $\rightarrow$ N_2(g), the desorbing (N-N) directly interacts with the metal surface. CO_2 is also repulsively desorbed along the surface normal, consistent with the results in the CO oxidation on Pd(110) [11]. On the other hand, the other products, ND_3 and D_2O are thermalized before desorption.

The precursor for the inclined N_2 emission is the lying N_2O(a) oriented along the [001] direction. The collimation of desorbing N_2 is determined by a repulsive force along the ruptured N-O bond and the interaction between desorbing N_2 and the surface. This scenario was already examined by DFT calculations, which predict that the main component of the reaction coordinate is along the N-O bond direction [17,20]. At the transition state, the calculated N-O distance is very close to the calculated reactant value [17]. The close distance between the O(a) and N_2 fragments at the transition state is the origin of the strong repulsion between the two fragments after the N-O bond is broken.

B. Kinetics relation

N_2O(a) is highly reactive on clean Pd(110) and decomposes even at around 100 K [4-6]. To keep its decomposition continuous, a reducing reagent is necessary to remove deposited oxygen. Its steady decomposition is controlled by either the reducing reagent adsorption or the dissociative N_2O adsorption. Below the kinetic transition point, the surface is covered by O(a) and the amount of CO(a) (or D(a)) is very small. The reducing reagent adsorption is rate-limiting, consistent with the first order in CO or D_2. Above the kinetic transition, the surface is covered by CO(a) and the amount of O(a) is very small because of the fast CO(a) + O(a) → CO_2(g) reaction. The surface above the kinetic transition is almost clean when D_2 is used. The N_2O adsorption or dissociation is rate-limiting, consistent with the negative order in CO or zero-th order in D_2. The angular and velocity distributions of desorbing N_2 remain invariant throughout this kinetic transition. These distributions (desorption dynamics) are merely controlled by the desorption process and not affected by the rate-determining step.

It is interesting that the desorption dynamics of N_2 in N_2O decomposition does not change when the surface species is switched from O(a) to CO(a) or even under adsorbate-free conditions. This also supports the occurrence of N_2O decomposition on clean parts of the surface. In fact, the active surface showed the (1×1) LEED pattern without super-structure spots. A Pd(110) surface is easily reconstructed into the well-known (1×3)-O, c(2×3)-1D-O or the c(4×2)-O structure when it is covered by different amounts of oxygen. This reconstruction is due to the (1×2) or (1×3) missing-row form stabilized by adsorbed oxygen, which is converted into the (1×1) non-reconstructed form when the oxygen is removed by CO or hydrogen above 360 K [9]. The N_2O reduction in the present work always proceeds above 400 K, and the surface structure is then merely controlled by O(a) and CO(a). The surface can provide clean (1×1) parts even below the kinetic transition point because of the small amount of adsorbed oxygen. The oxygen level must be below the 1/4 monolayer except for very low CO pressures because the sticking probability of N_2O dissociative adsorption decreases below 0.1 above 400 K [16]. In fact, the decomposition of N_2O is severely retarded by the presence of O(a) [6,21].

The kinetic transition of the NO + CO (or D_2) reaction is not as clear as that of the N_2O reduction. At 550 K, with increasing P_{CO}, the N_2 signal at 40° increased steeply with a slope of 1.8 and reached a steady level above the ratio of $P_{CO}/P_{NO} = 0.7$. N_2 was merely desorbed into the inclined way over a wide CO pressure range. The overall reaction was controlled by the NO dissociation. This dissociation was affected by surface oxygen when the reaction was highly sensitive to CO. After reaching the steady level, the NO dissociation was affected by CO(a). On the other hand, at 640 K, the N_2 desorption was fairly inclined at low P_{CO}. At high P_{CO}, the N_2 signal at $\theta = 0°$ was enhanced, i. e., the desorption including the normally directed and cosine components became dominant.

Process (ii) N_2O(a) → N_2(g) + O(a) on a clean Pd(110) is insensitive to the surface temperature [6]. The steep enhanced N_2O reduction observed below 500 K (Fig. 5) is due to the removal of CO(a). The rate rapidly decreased after the maximum because of the decreased sticking probability of N_2O. On the other hand, the steep increased NO reduction around 500 K (Fig. 2) is due to enhanced NO dissociation. At higher temperatures, process (i) 2N(a) → N_2(g) becomes predominant because of the higher activation energy.

C. Other surfaces and perspectives

It should be noted that the decomposition of adsorbed N_2O is sensitive to the surface structure. The N_2O species is very reactive on open surfaces, such as Cu(110), stepped Ni(557), Ni(110), Ni(100), Rh(110), and Ir(110).[21-27] The decomposition proceeds at around 100 K, as described on Pd(110), or even below it. Thus, it is reasonable that its steady-state decomposition with a suitable reducing reagent is controlled by either the N_2O dissociative adsorption or the deposited oxygen removal. In other words, ordinary kinetic measurements at the steady state are not informative for the removal processes of N_2O(a). On the other hand, the reaction pathway through the N_2O intermediate is not operative in the deNOx process toward N_2 on Pt(111), Rh(111), and Ir(111) because no N_2O is decomposed on these surfaces although it is easily formed from N(a)+NO(a) on them.[28-31] On real catalysts involving fine metal particles, there are many different surface planes, which show their own reactivity as well as their own pathways. Each plane may contribute from their unique processes, and the overall reaction eventually proceeds after several planes work cooperatively. Here, the surface transport of N_2O between different planes will play an essential role in the total selectivity.

Product desorption from catalyst surfaces is the final process of surface chemical reactions. Its properties must be consistently characterized from both chemical kinetics and reaction dynamics. Kinetics is concerned with the desorption frequency (reaction rate), and dynamics deals with the energy partition during an event.[32] AR-product desorption analysis is informative toward surface-nitrogen removal processes because of the different angular distribution in each removal step. Velocity distributions help the above AR-product desorption analysis on flat surfaces, whereas, on complex surfaces, such as metal particles supported on oxides, the velocity distribution may provide information about involved pathways more than the angular distribution. Analyzing desorbing products in state-resolved ways will yield direct evidence of the presence of processes yielding products with hyper-thermal energy.[33] The relaxation time of vibrationally excited molecules is very short, in the order of 10^{-12} s on metal surfaces.[34] In fact, the fragment product being desorbed has been believed to be thermalized to the surface temperature before emission. The inclined N_2 emission from the N_2O decomposition is the first example of the collimated fragment desorption in thermal decompositions.[32] Such desorption with hyper-thermal energy will be found in thermal decompositions on nano-sized particles because of the delayed energy relaxation. Energy analysis of desorbing products from nano-particles would be worthwhile.

V. **Conclusions**

The reaction pathways of NO reduction on Pd(110) were studied from the angular and velocity distributions of desorbing products in the course of catalyzed NO and N_2O reduction. At temperatures below 600 K, processes (ii) $N_2O(a) \rightarrow N_2(g) + O(a)$ and (iii) $N_2O(a) \rightarrow N_2O(g)$ dominate and process (iv) $N(a) + 3H(a) \rightarrow NH_3(g)$ is enhanced at H_2 pressures higher than NO. Process (i) $2N(a) \rightarrow N_2(g)$ contributes significantly above 600 K. Only process (ii) was observed in a steady-state $N_2O + CO$ (or H_2) reaction.

Acknowledgements

The authors thank Professor V. P. Zhdanov (Boreskov Research Institute for Catalysis) and Dr. A. Kokalj (J. Stefan Institute) for their stimulating discussion and Ms. Hiratsuka for drawing the figures. This work was partly supported by a 1996 COE special equipment program of the Ministry of Education, Sports, and Culture of Japan.

References

[1] T. Matsushima, Surf. Sci. Rep., 52 (2003) 1.
[2] T. Matsushima, Surf. Sci., 197 (1988) L287. .
[3] M. Ikai and K. I. Tanaka, J. Phys. Chem. B 103 (1999) 8277.
[4] Y. Ohno, K. Kimura, M. Bi and T. Matsushima, J. Chem. Phys., 110 (1999) 8221.
[5] Y. Ohno, I. Kobal, H. Horino, I. I. Rzeznicka and T. Matsushima, Appl. Surf. Sci., 169/170 (2001) 273.
[6] H. Horino, S. Liu, A. Hiratsuka, Y. Ohno and T. Matsushima, Chem. Phys. Lett., 341 (2001) 419.
[7] M. Kobayashi and Y. Tuzi, J. Vac. Sci. Technol., 16 (1979) 685.
[8] I. I. Rzeznicka, Y. -S. Ma, G.. Cao and T. Matsushima, J. Phys. Chem. B 108 (2004) 14232.
[9] I. I. Rzeznicka, and T. Matsushima, Chem. Phys. Lett., 377 (2003) 279.
[10] T. Matsushima, C. J. Mussett and J. M. White, J. Catal., 41 (1976) 397.
[11] Md. G.. Moula, S. Wako, G.. Cao, K. Kimura, Y. Ohno, I. Kobal and T. Matsushima, Phys. Chem. Chem. Phys., 1 (1999) 3677.
[12] J. W. He, U. Memmert and P. R. Norton , J. Chem. Phys., 90 (1989) 5082.
[13] E. Ozensoy, C. Hess and D.W. Goodman, J. Am. Chem. Soc., 124 (2002) 8524.
[14] E. Ozensoy and D.W. Goodman, Phys. Chem. Chem. Phys., 6 (2004) 3765.
[15] N. V. Richardson and N. Sheppard, in: *Vibrational Spectroscopy of Molecules on Surfaces*, eds. by J. T. Yates Jr. and T. E. Madey (Plenum Press, New York, 1987) p 1.
[16] S. Haq and A. Hodgson, Surf. Sci., 463 (2000) 1.
[17] A. Kokalj, I. Kobal and T. Matsushima, J. Phys. Chem. B 107 (2003) 2741.
[18] H. Horino, I. I. Rzeznicka, T. Matsushima, K. Takahashi and E. Nakamura, *UVSOR Activity Report* (2002) 2003, p209.
[19] K. Watanabe, A. Kokalj, Y. Inokuchi, I. Rzeznicka, K. Ohshimo, N. Nishi and T. Matsushima, Chem. Phys. Lett., 406 (2005) 474.
[20] I. Kobal, A. Kokalj, H. Horino, Y. Ohno and T. Matsushima, Trends in Chem Phys., 10 (2002) 139.
[21] T. Matsushima, K. Imamura, H. Horino, A. Hiratsuka, Y.-S. Ma, I. I. Rzeznicka and O. Nakagoe, Appl. Surf. Sci., 244 (2005) 141.
[22] H. Horino, I. I. Rzeznicka, A. Kokalj, I. Kobal, A. Hiratsuka, Y. Ohno and T. Matsushima, J. Vac. Sci. Technolog. A 20 (2002) 1592.
[23] A. Spitzer and H. Lüth, Phys. Rev. B 30 (1984) 3098.
[24] C. Kodama, H. Orita and H. Nozoye, Appl. Surf. Sci., 121/122 (1997) 579.
[25] R. Sau and J. B. Hudson, J. Vac. Sci. Technol., 18 (1981) 607.
[26] D. A. Hoffman and J. B. Hudson, Surf. Sci., 180 (1987) 77.
[27] Y. Li and M. Bowker, Surf. Sci., 348 (1996) 67.
[28] N. R. Avery, Surf. Sci., 131 (1983) 501.
[29] J. C. L. Cornish and N. R. Avery, Surf. Sci., 235 (1990) 209.
[30] D. N. Belton, C.L. DiMaggio, S. L. Sxchmieg and K.Y. Simon Ng, J. Catal., 157 (1995) 559.
[31] H. Wang, R. G. Tobin, C. L. DiMaggio, G. B. Fisher and D. K. Lambert, J. Chem. Phys., 107 (1997) 9569.

[32] T. Matsushima, I. I. Rzeznicka and Y.-S. Ma, Chem. Record., 5 (2005) 81.
[33] A. Hodgson, Prog. Surf. Sci., 63 (2000) 1.
[34] E. J. Heiweil, M. P. Casassa, R. R. Cavanagh and J. T. Stephensen, Ann. Rev. Phys. Chem., 40 (1989) 143.

Figure Captions

Fig. 1 Principle behind the apparatus for angle-resolved product desorption measurements with time-of-flight techniques. The inserts show the shape of the chopper blade and the structure around a sample crystal and a gas doser. QMS (quadrupole mass spectrometer); MCS (multi-channel scalar); trigger (photocell and light-emitting diode). The chopper house was pumped at about 7 m^3s^{-1}. A top view of Pd(110) and its crystal azimuths are shown on the bottom.

Fig. 2 Surface temperature dependence of the AR product signals at their collimation angles in a steady-state $^{15}NO + D_2$ reaction. The ^{15}NO pressure was 5×10^{-6} Torr and the pressure ratio of $^{15}NO/D_2$ was 2. The spatial distribution of desorbing products in each process is inserted on the right-hand side.

Fig. 3 (a,b) Angular and (c,d) velocity distributions of desorbing $^{15}N_2$ at different T_S and θ values in the steady-state $^{15}NO + D_2$ reaction under the condition in Fig. 2. Typical deconvolutions are given by broken curves. The translational temperature of each component is inserted. The desorption angle θ and the intensity presentation are drawn in the upper panel.

Fig. 4 Angular and velocity distributions of desorbing (a) $^{15}ND_3$ at T_S = 550 K in the steady-state $^{15}NO + D_2$ reaction at $P_{15NO} = 5\times10^{-6}$ Torr and $P_{D2} = 1.3\times10^{-5}$ Torr, (b) $^{13}CO_2$ at T_S = 470 K in the steady-state $^{15}N_2O + {}^{13}CO$ reaction at $P_{15N2O} = 3.3\times10^{-6}$ Torr and $P_{13CO} = 0.3\times10^{-6}$ Torr, and (c) D_2O at T_S = 470 K in the steady-state $^{15}N_2O + D_2$ reaction at $P_{15N2O} = 3.3\times10^{-6}$ Torr and $P_{D2} = 0.5\times10^{-6}$ Torr. The velocity distributions at the normal direction are shown. Typical deconvolutions for CO_2 are given by broken curves. The translational temperature of each component is inserted.

Fig. 5 Surface temperature dependence of the AR product signals at their collimation angles in a steady-state $^{15}N_2O$ reduction by (a) D_2 and (b) CO. $^{15}N_2O$, 3.3×10^{-6} Torr, D_2 or CO, 0.5×10^{-6} Torr.

Fig. 6 Angular and velocity distributions of desorbing $^{15}N_2$ in the steady-state $^{15}N_2O + D_2$ reaction at $P_{15N2O} = 3.3\times10^{-6}$ Torr and $P_{D2} = 0.5\times10^{-6}$ Torr at T_S = (a) 410 K and (b) 750 K . Typical deconvolutions are given by broken curves. The translational temperature of each component is inserted. The desorption angle θ and the intensity presentation are drawn in the upper panel.

Fig. 7 P_{CO} and P_{D2} dependence of the AR-$^{15}N_2$ signal at the collimation angle at different T_S values in a steady-state $^{15}N_2O$ reduction by (a) CO and (b) D_2. $P_{N2O} = 3.3\times10^{-6}$ Torr. A kinetic transition is drawn by the vertical lines.

Angular distributions of desorbing N_2 in the $^{15}N_2O + CO$ reaction below and above the kinetic transition at 470 K are shown. Very similar angular distributions of $^{15}N_2$ were also observed in the $^{15}N_2O + D_2$ reaction.

Fig. 8 (a) Transient $^{15}N_2$ and $^{13}CO_2$ formation curves after stopping of the ^{13}CO supply from the steady-state $^{15}N_2O + CO$ reaction at $P_{N2O} = 3.3\times10^{-6}$ Torr and $P_{CO} = 0.5\times10^{-6}$ Torr in the inhibited region at $T_S = 470$ K. (b) Transient N_2 formation after stopping of the D_2 supply from the steady-state $N_2O + D_2$ reaction at $P_{N2O} = 3.3\times10^{-6}$ Torr and $P_{D2} = 0.5\times10^{-6}$ Torr. $T_S = 470$ K. The decays of the AI ^{13}CO and D_2 signals are also shown. The cross-hatched areas show the amount of N_2 formation on a clean surface without removal of O(a).

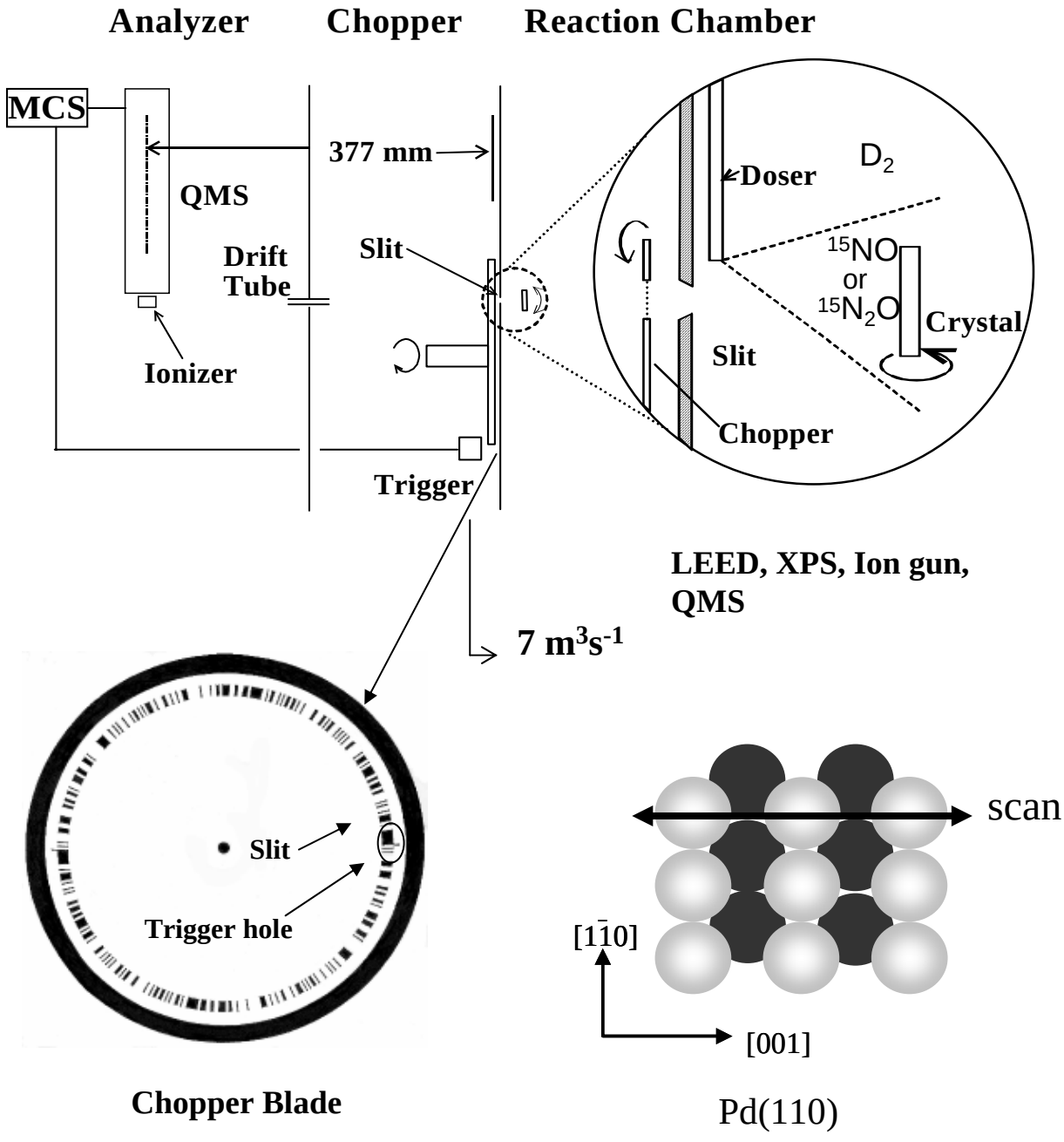
Analyzer
Chopper
Reaction Chamber
MCS
QMS
Drift Tube
Ionizer
377 mm
Slit
Trigger
Doser
D_2
^{15}NO or $^{15}N_2O$
Crystal
Slit
Chopper
LEED, XPS, Ion gun, QMS
7 m^3s^{-1}
Slit
Trigger hole
Chopper Blade
scan
[1$\bar{1}$0]
[001]
Pd(110)

Fig. 1 Ma

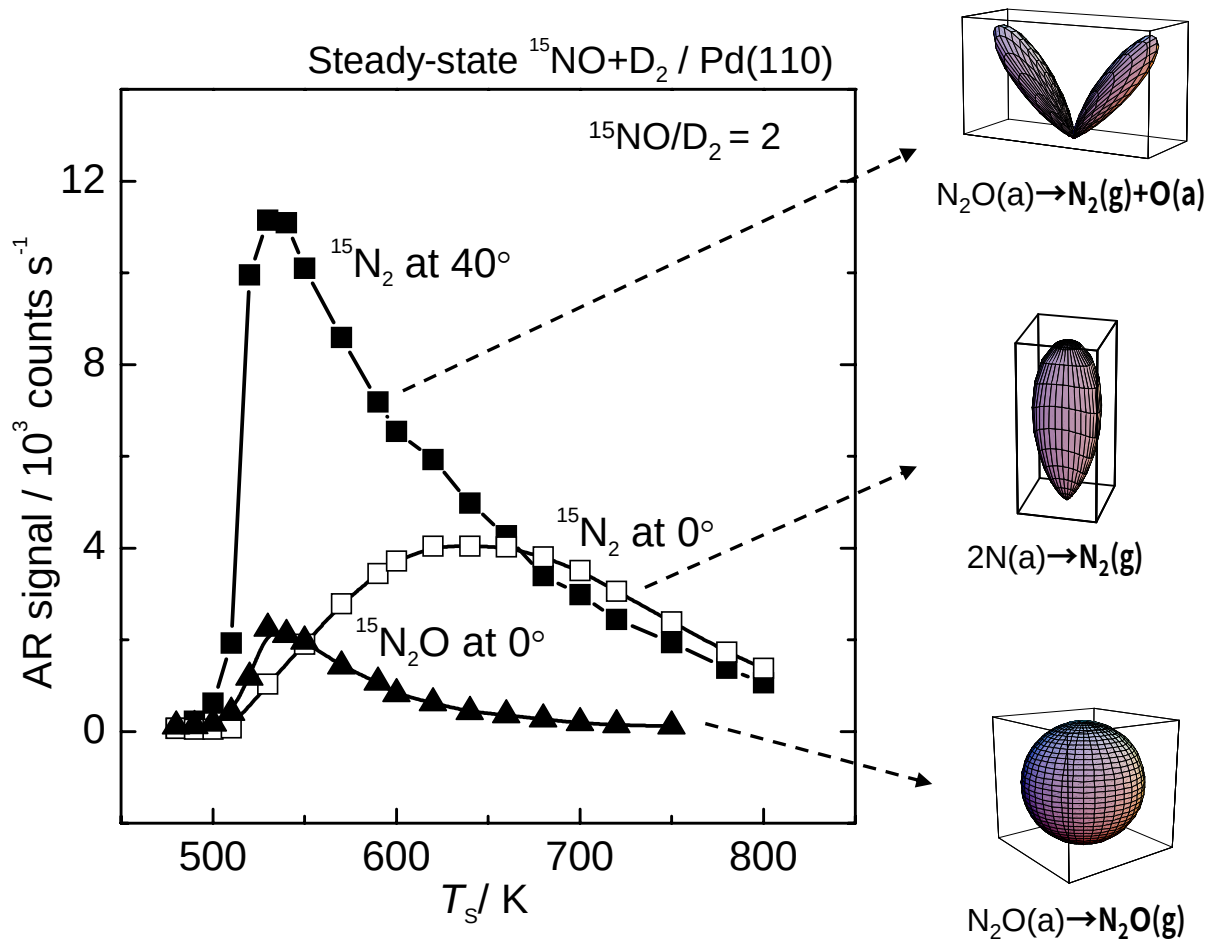
Steady-state $^{15}NO+D_2$ / Pd(110)
$^{15}NO/D_2 = 2$
$^{15}N_2$ at 40°
$^{15}N_2$ at 0°
$^{15}N_2O$ at 0°
AR signal / 10^3 counts s^{-1}
T_S/ K
$N_2O(a) \rightarrow \mathbf{N_2(g)+O(a)}$
$2N(a) \rightarrow \mathbf{N_2(g)}$
$N_2O(a) \rightarrow \mathbf{N_2O(g)}$

Fig. 2 Ma

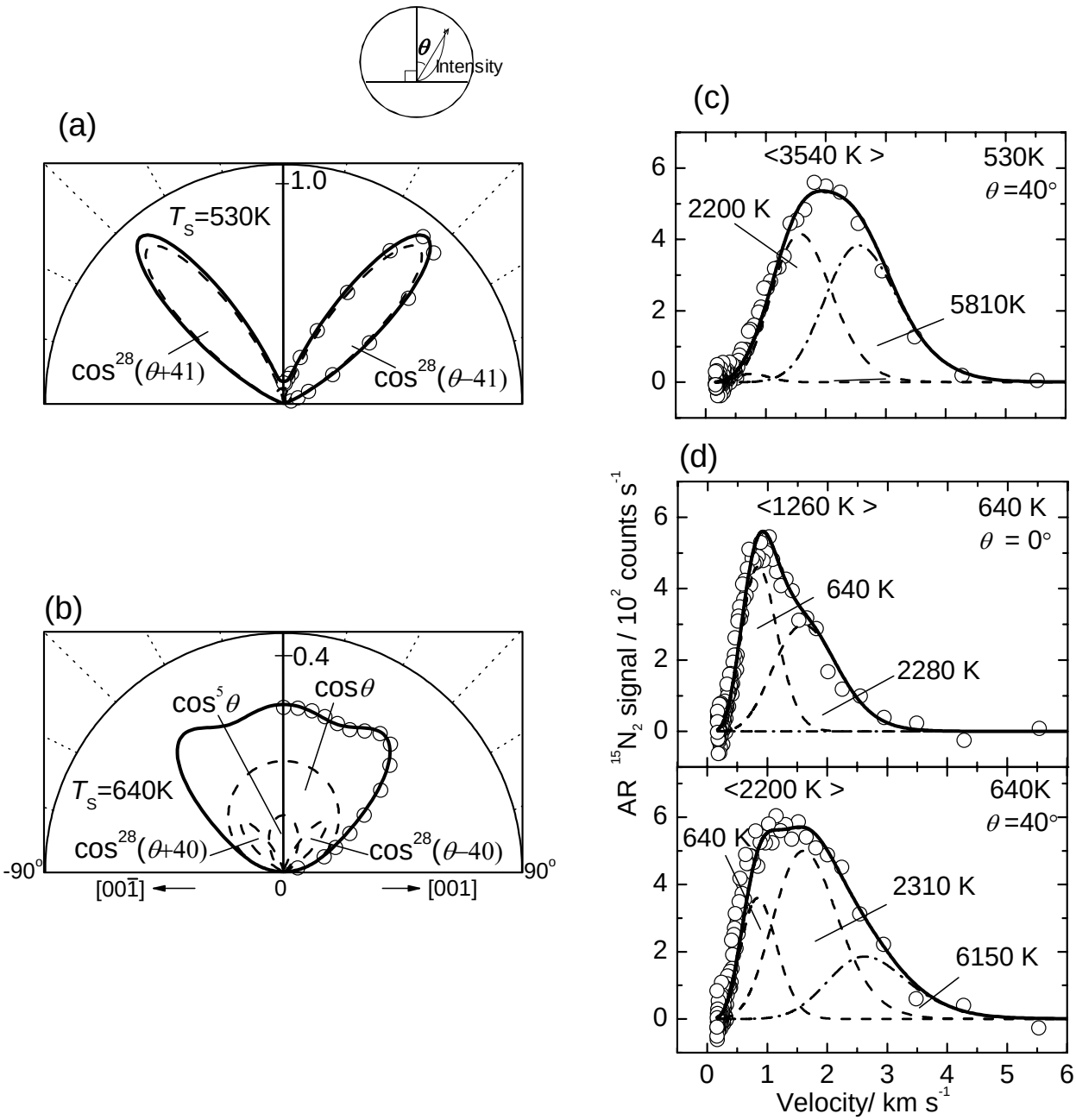
θ
Intensity
(a)
1.0
T_S=530K
cos^{28}(θ+41)
cos^{28}(θ–41)
(b)
0.4
cos^{5}θ
cosθ
T_S=640K
cos^{28}(θ+40)
cos^{28}(θ–40)
-90°
90°
[00$\bar{1}$]
0
[001]
(c)
<3540 K >
530K
θ =40°
2200 K
5810K
(d)
<1260 K >
640 K
θ = 0°
640 K
2280 K
<2200 K >
640K
θ =40°
640 K
2310 K
6150 K
AR $^{15}N_2$ signal / 10^2 counts s^{-1}
Velocity/ km s^{-1}

Fig.3 Ma

(a) $^{15}ND_3$ in $^{15}NO+D_2$

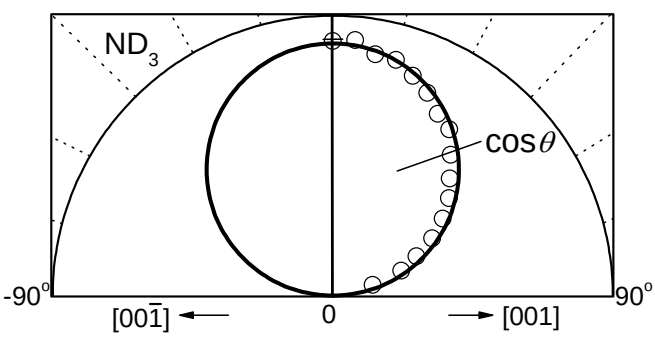

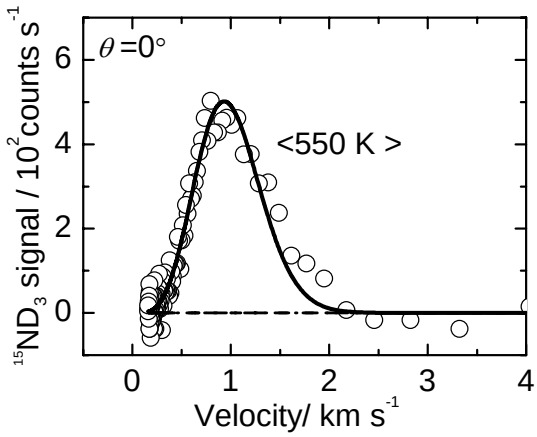

(b) $^{13}CO_2$ in $^{15}N_2O+^{13}CO$

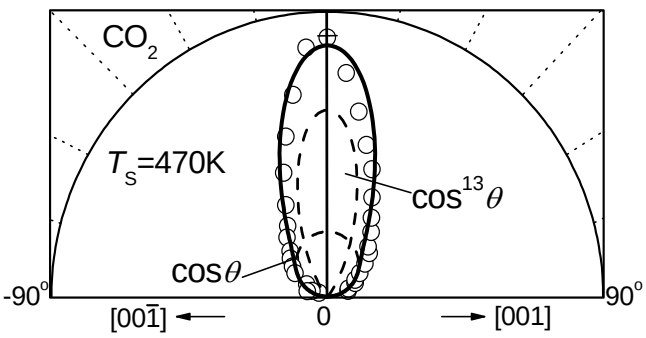

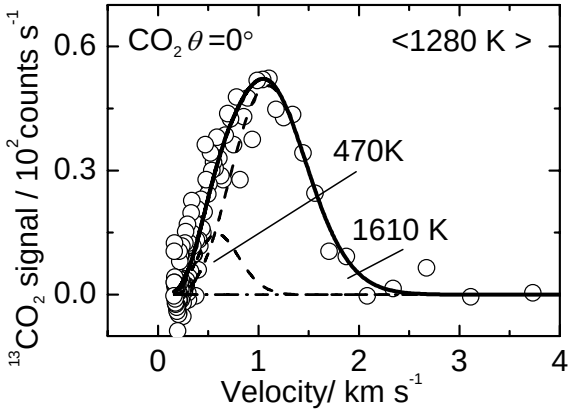

(c) D_2O in $^{15}N_2O$ +D_2

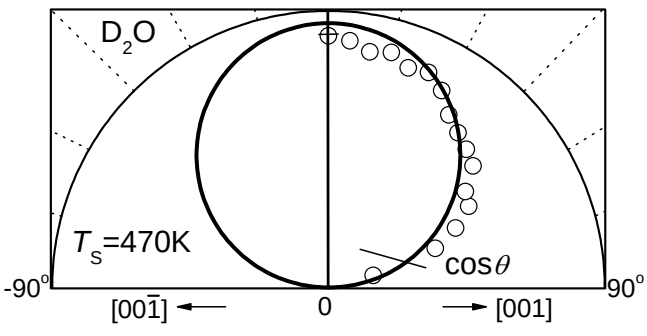

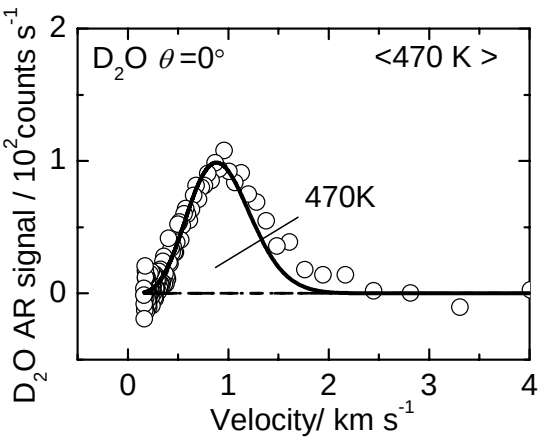

Fig.4 Ma

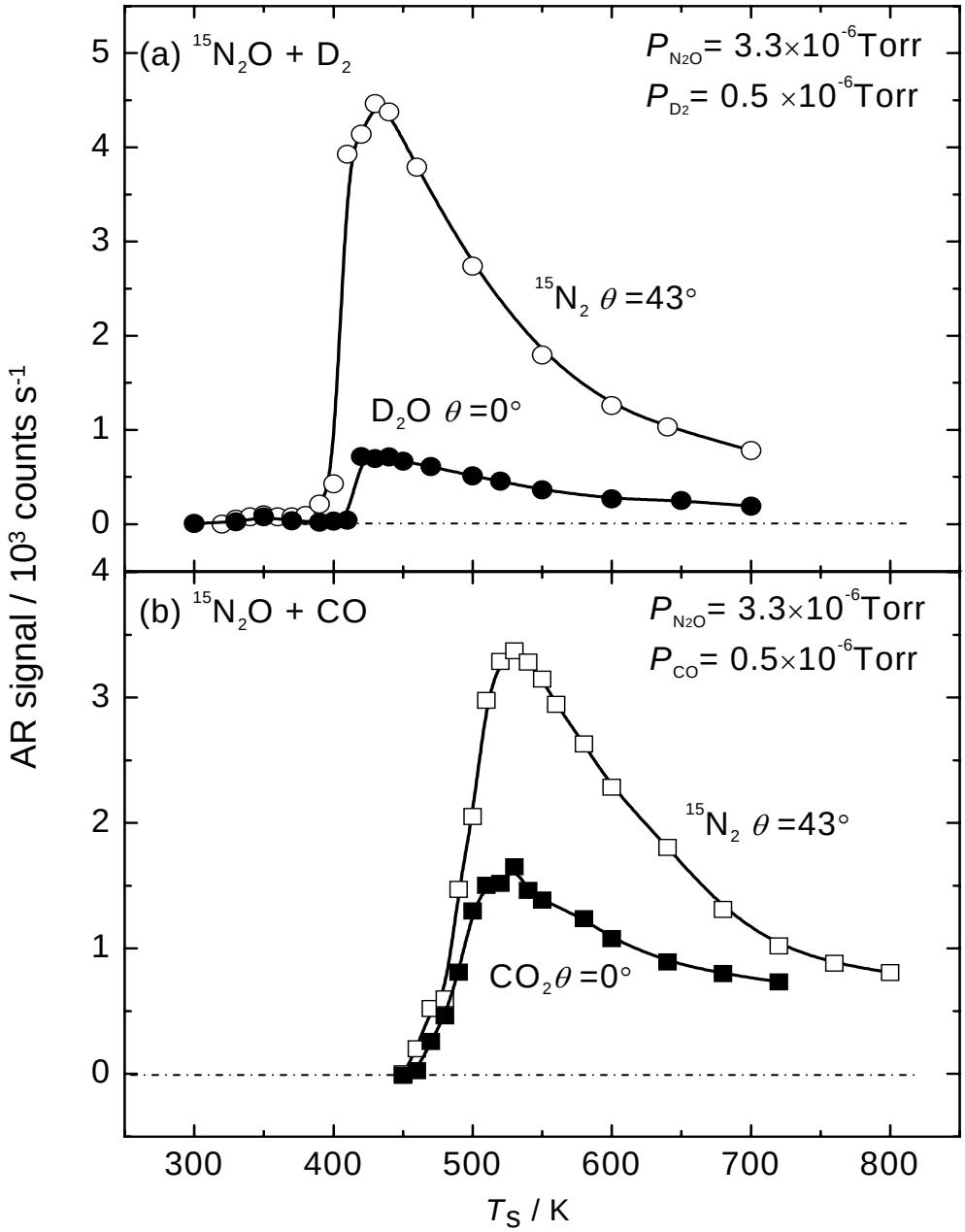
(a) $^{15}N_2O + D_2$
P_{N2O}= 3.3×10^{-6}Torr
P_{D2}= 0.5 ×10^{-6}Torr
$^{15}N_2$ θ =43°
D_2O θ =0°
(b) $^{15}N_2O$ + CO
P_{N2O}= 3.3×10^{-6}Torr
P_{CO}= 0.5×10^{-6}Torr
$^{15}N_2$ θ =43°
CO_2θ =0°
AR signal / 10^3 counts s^{-1}
T_S / K

Fig.5 Ma

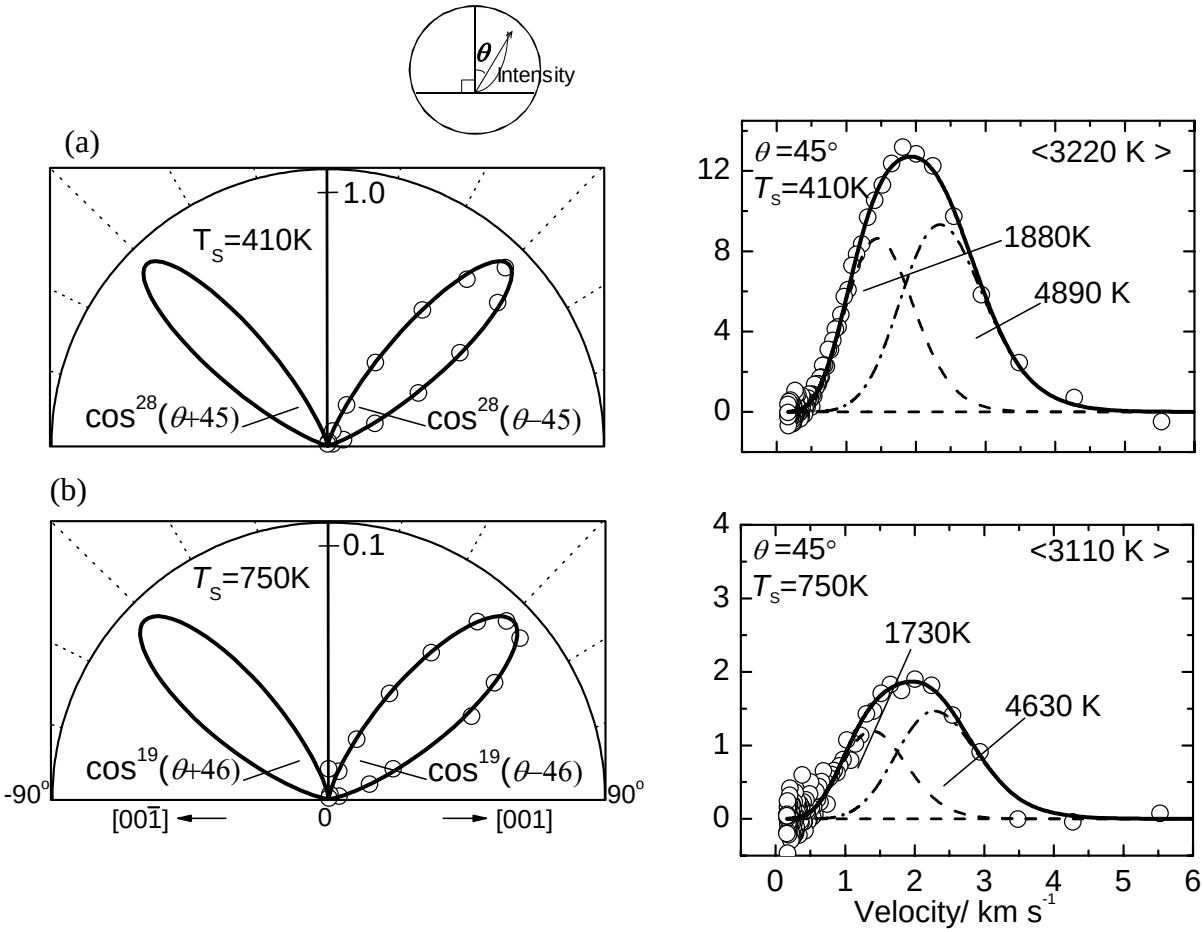
θ
Intensity
(a)
1.0
T_S=410K
cos^28(θ+45)
cos^28(θ–45)
θ=45°
T_S=410K
<3220 K >
1880K
4890 K
(b)
0.1
T_S=750K
cos^19(θ+46)
cos^19(θ–46)
-90°
90°
[00$\bar{1}$]
0
[001]
θ=45°
T_S=750K
<3110 K >
1730K
4630 K
Velocity/ km s^-1

Fig6. Ma

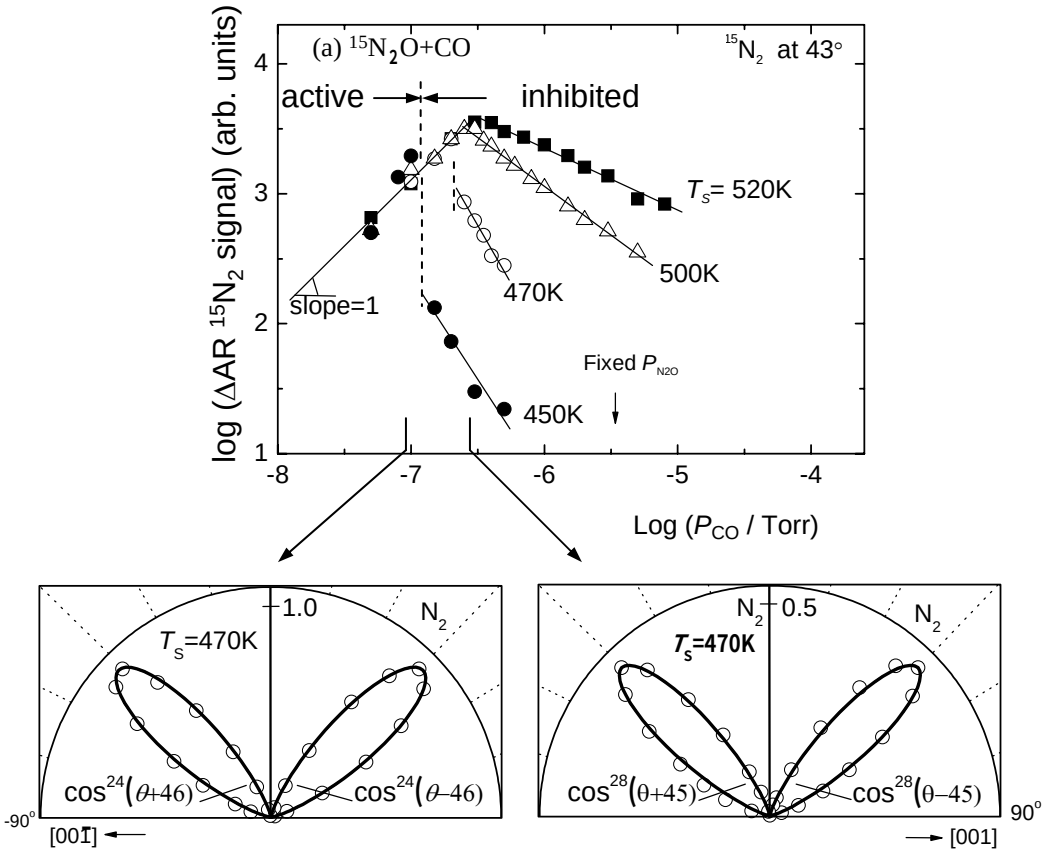
(a) $^{15}N_2O$+CO
$^{15}N_2$ at 43°
active
inhibited
T_S= 520K
500K
470K
450K
slope=1
Fixed P_{N2O}
log (ΔAR $^{15}N_2$ signal) (arb. units)
Log (P_{CO} / Torr)
T_S=470K
1.0
N_2
$\cos^{24}(\theta+46)$
$\cos^{24}(\theta-46)$
-90°
[00$\bar{1}$]
N_2 0.5
T_S=470K
$\cos^{28}(\theta+45)$
$\cos^{28}(\theta-45)$
90°
[001]

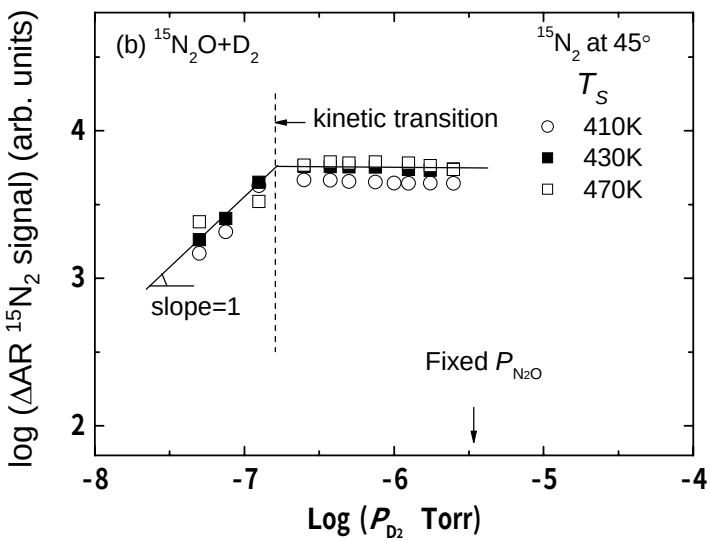
(b) $^{15}N_2O$+D_2
$^{15}N_2$ at 45°
T_S
410K
430K
470K
kinetic transition
slope=1
Fixed P_{N2O}
log (ΔAR $^{15}N_2$ signal) (arb. units)
Log (P_{D_2} Torr)

Fig.7 Ma

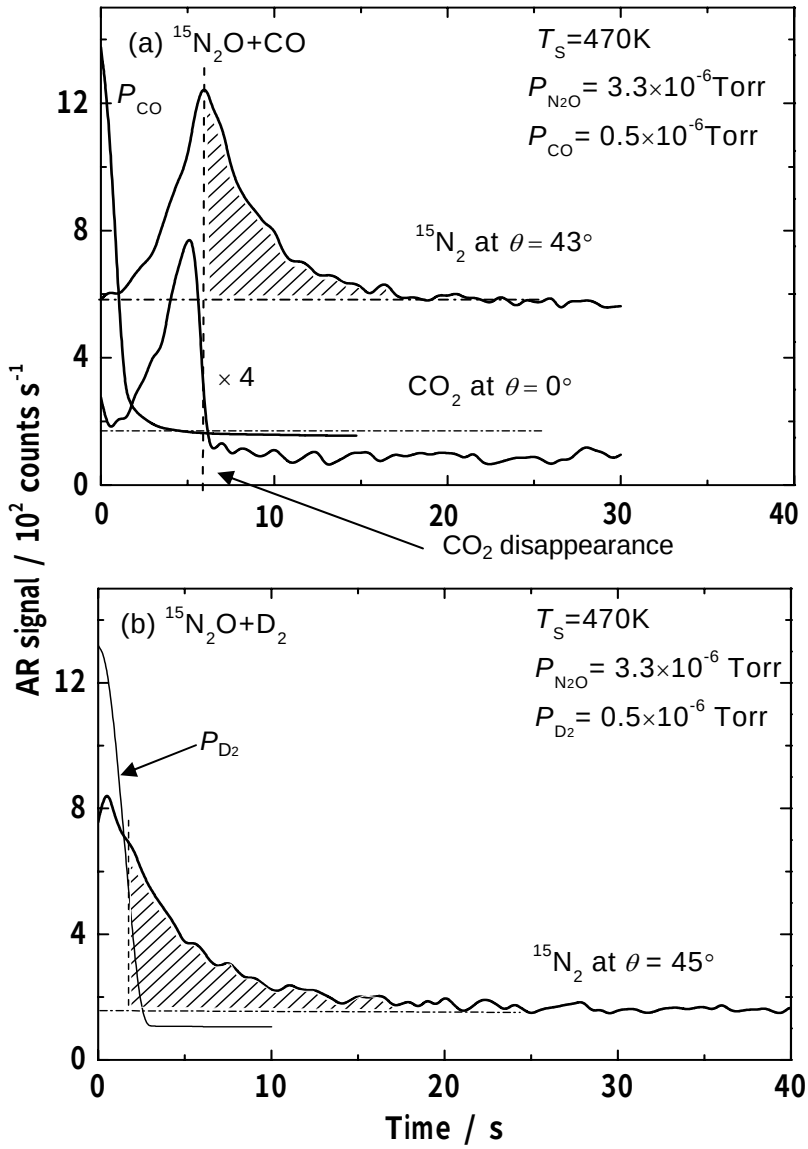
(a) $^{15}N_2O$+CO
T_S=470K
P_{N2O}= 3.3×10^{-6}Torr
P_{CO}= 0.5×10^{-6}Torr
P_{CO}
$^{15}N_2$ at θ = 43°
× 4
CO_2 at θ = 0°
CO_2 disappearance
(b) $^{15}N_2O$+D_2
T_S=470K
P_{N2O}= 3.3×10^{-6} Torr
P_{D2}= 0.5×10^{-6} Torr
P_{D2}
$^{15}N_2$ at θ = 45°
AR signal / 10^2 counts s^{-1}
Time / s
0
4
8
12
0
10
20
30
40

Fig.8 Ma